Journal of
Nanoscience and Nanotechnology
Vol. 7, 1–9, 2007

Adaptive Brownian Dynamics for Shape Estimation of Sodium Ion Channels

Vikram Krishnamurthy[1,*], Taira Vora[2], and Shin-Ho Chung[3]

[1] *Department of Electrical and Computer Engineering, University of British Columbia, Vancouver, V6T 1Z4, Canada*
[3] *Department of Theoretical Physics, Research School of Physical Sciences, The Australian National University, Canberra, ACT 0200, Australia*

Ion channels are protein macromolecules that form biological nanotubes across the membranes of living cells. Given many possible geometrical shapes of an ion channel, we propose a computational scheme of selecting the model that best replicates experimental observations, using adaptive Brownian dynamics simulations together with discrete optimization algorithms. Brownian dynamics simulations emulate the propagation of individual ions through the sodium ion channel nanotube at a femto time second time scale and Angstrom unit (10^{-10} meter) spatial scale.

Keywords:

1. INTRODUCTION

Ion channels are biological nanotubes formed by protein macromolecules residing within the cell membrane of all living organisms. They regulate all electrical activities of a cell by controlling the passage of ions into and out of the cell, thus maintaining the resting membrane potentials and, when needed, causing the generation and propagation of action potentials. Understanding the structure and dynamics of ion channels is a fundamental problem in biology. It is now known that genetic alterations of some of the genes synthesizing channel proteins are known to be associated with many inherited disorders, such as epilepsy, muscular disorders, cystic fibrosis, and diabetes.[8] Elucidation of how single ion channels work will ultimately help neurobiologists find the causes of, and possibly cures for, a number of neurological and muscular disorders.

Recently the structures of several bacterial ion channels have been determined by crystallographic analyses.[5,6] These discoveries have led to several recent papers where *Brownian dynamics modelling* and *Brownian dynamics simulations* of ion channels have been used to unravel structural properties of similar ion channels. Brownian dynamics (BD) modelling of an ion channel captures the dynamics of ions both within the ion channel and in the vicinity of the ion channel as a large scale interacting particle stochastic dynamical system. The modeling method deals with the computer simulation of this large scale stochastic dynamical system at an Å spatial scale and femto-second time scale resolution. The dynamics (velocity) of individual ions of this large scale stochastic dynamical system evolve according to a large dimensional vector stochastic differential equation called the Langevin equation. The Langevin equation also takes into account of systematic forces acting on ions within the nanotube of the ion channel—these systematic forces are a function of the structure of the ion channel, such as charge of amino acids lining the inner wall of the ion channel and the three dimensional shape of the channel. Thus the average time taken for an ion to cross the ion channel depends on these structural properties. It logically follows that by optimizing the fit between the Brownian dynamics simulated ion channel current (charge per unit time) and the experimentally measured ion channel currents, one can estimate the structural properties of an ion channel. This is the underlying idea of the paper.

The key idea in this paper is to derive a novel discrete stochastic approximation based algorithm to dynamically control the behaviour of the BD simulation. The resulting algorithm yields the optimal estimate of the shape of an ion channel by optimizing the match between the BD simulated ion channel current and experimentally determined current. By using a parameterized structure, we formulate the problem of estimating the shape of an ion channel the discrete stochastic optimization problem.

The paper is organized as follows. We begin by formulating the BD algorithm to calculate currents through ion channels. We then discuss the optimization algorithms devised to search and converge on the optimal shape of the pore for sodium channels. We then provide a numerical analysis of the performance of our algorithms.

*Author to whom correspondence should be addressed.

RESEARCH ARTICLE

2. SODIUM ION CHANNEL MODEL AND BROWNIAN DYNAMICS ION PERMEATION MODEL

2.1. Construction of Sodium Ion Channel Structural Model

The aim of this subsection if to carefully construct a finite number of feasible structural shapes for a sodium ion channel. These feasible shapes need to capture the following unique properties of the sodium ion channel. First, the sodium ion channel allows over 10^6 ions through the channel every second, and yet is able to distinguish between sodium and other ions. Second, it has a high affinity for monovalent ions, is rapidly blocked by divalent ions and allows no anions through. Third, the channel exhibits a symmetric, linear current–voltage curve when there is symmetric concentrations of NaCl in the intracellular and extra-cellular regions, and the current rapidly saturates with increasing concentrations. Finally, the channel is completely blocked when divalent ions are present in the external solution, but only marginally reduced in presence of intracellular divalent ions.

In order to model the sodium ion channel, and due to the lack of data available on its atomic structure, feasible models for the sodium channel must take into account the above properties and successfully reproduce available experimental current–voltage and current–concentration responses of the channel.

A sodium ion channel comprises of four functional components: external vestibule, selectivity filter, internal pore, and internal entrance region. The family of sodium ion channels are believed to be structurally similar to the family of potassium ion channels. Thus, we have based the feasible shapes of the sodium channel on the KCsA potassium channel, the structure of which was recently crystallized by Doyle et al.[5] We have shortened the selectivity filter and added an external vestibule to the existing potassium channel shape. Below we describe in detail how by carefully varying the dimensions of the above structural components there are a finite number of distinct possibilities for the shape. The candidate channels are depicted in Figure 1 and the various parameters of these candidate channels are given in Table I

(i) *Outer vestibule*: The outer regions making up the sodium channel protein are believed to be composed of the P loops of the protein that form a conical outer vestibule.[8, 15]

(ii) *Selectivity filter*: Similar to the KCsA, we include a short selectivity filter followed by an internal pore region. All channel models contain a selectivity filter with a radius of $r = 2.2$ Å derived from permeant cation studies by Hille.[10] As the length of the filter is unknown, we vary this parameter to fit the current. We use only the two charged rings suspected to lie in the selectivity filter, and known from mutation studies to have a large effect on selectivity and conductance of the sodium channel.[9, 19, 21] The two charged rings are placed around the filter region as point charges, 1 Å behind the protein boundary, at a distance of $z = 14$ Å and $z = 18.5$ Å from the central axis of the channel. The inner ring contains a positively charged lysine and a negatively charged glutamate and aspartate amino acid group, and the outer ring contains two negatively charged glutamates and two negatively charged aspartates. The positive lysine in the inner ring is fully charged, but we believe that more than one negative residue is likely to be protonated. For the position and charged states of these residues we have used the data of Ref. [22]. They find that two residues must be protonated at any given time to reproduce the experimental data. The inner ring has a total charge of -1.0×10^{-19} C on average, where the lysine has the charge of one proton, and the negative residues in the inner ring a charge of -1.3×10^{-19} C each. The outer ring contains a total charge of 3.8×10^{-19} C where the total charge is shared equally among all four negative residues, giving each residue a charge of 0.95×10^{-19} C. We distribute equal charges among all residues in a ring because the exact charge state of any residue at a given time is difficult to calculate, only the average behaviour of the charged residue can be estimated.

(iii) *Inner pore:* Followed by the selectivity filter is an inner vestibule region. This is again adopted from the KcsA structure. The diameter and length of this region is unknown and has been varied in the shape estimation of the channel.

(iv) *Internal entrance:* The internal entrance leads into the inside of the cell. This region contains the carboxyl end of the protein making up the sodium channel. For this reason we include a set of dipole charges at $z = -20$ Å, mimicking the intracellular helix dipoles of the channel protein. The magnitude of charge on the helix dipoles is 0.6×10^{-19} C. The negative end is nearer to the channel entrance, the positive ends are buried deep inside the protein and its effect is negligible.

The channel model is generated by creating an initial outline of the channel pore and then rotating it by 180 °C to create a three-dimensional shape. Cylindrical symmetry is assumed with the channel centered around $z = 0$ Å and extending out to $z = \pm 27$. An extracellular and intracellular reservoir, $\mathscr{R}_1$ and $\mathscr{R}_2$, is attached to either ends of the channel. The channel model has been varied systematically, all shapes used are given in Figure 1 and Table I. On the above stated basic outline (of outer vestibule, selectivity filter, inner pore and internal entrance), we have varied the dimensions of the channel to obtain currents through each individual channel. The parameters that were varied are stated in Table I. We have varied the width and height of the outer vestibule (shapes 1 and 2), length of the selectivity filter (shapes 3 and 4), width of the inner pore (shape 5), and the width of the intracellular pore (shapes 4, 6, and 7) and the width, and height of the outer vestibule

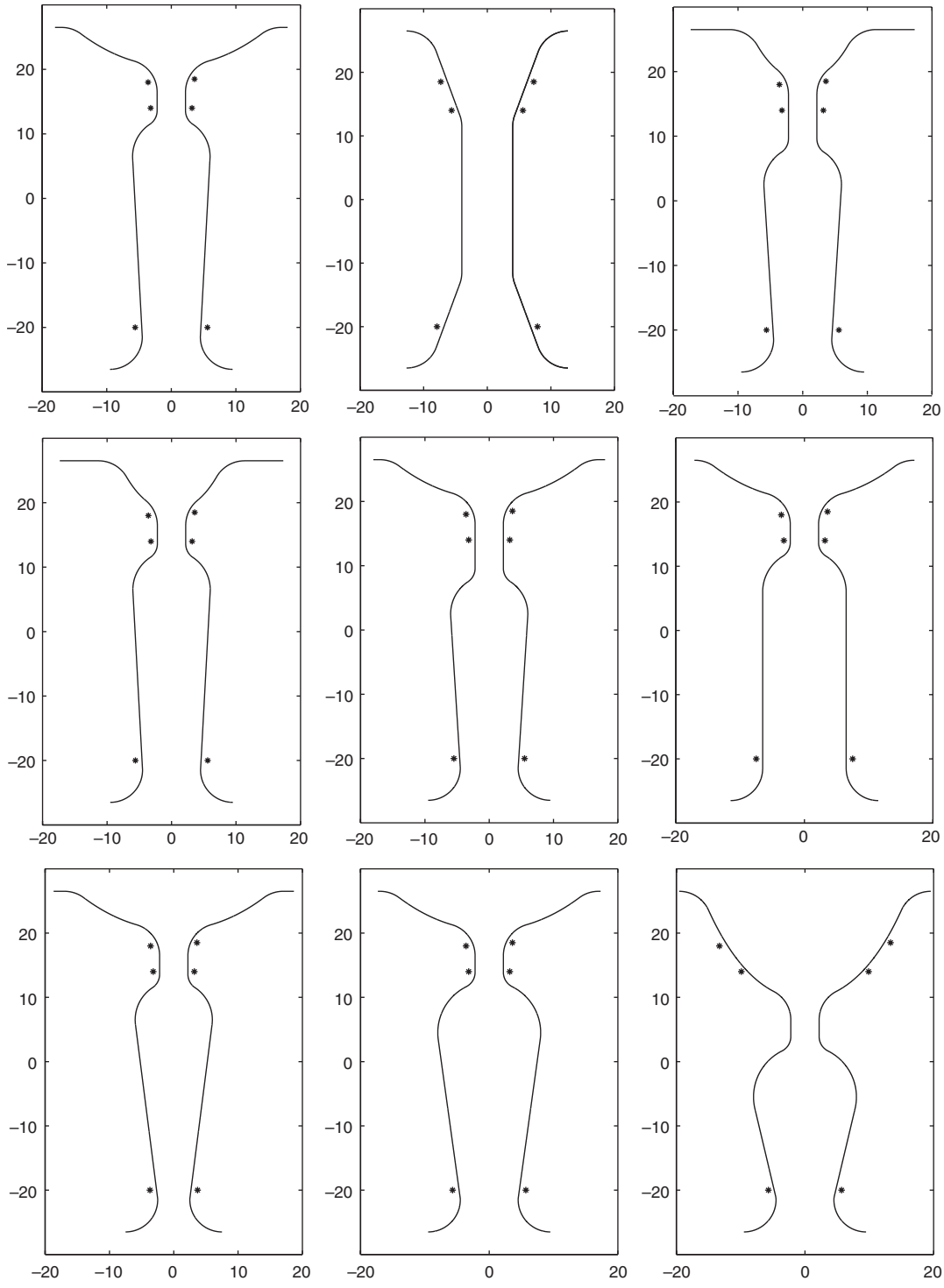

Fig. 1. Nine candidate channel shapes for the sodium ion channel nanotube considered in this paper. The 6 dots in each figure denote point charges in the protein lining the inner wall of the nanotube—all units are in angstrom units Å (1 Å $= 10^{-10}$ m). The upper four dots represent the point charge approximations of the two charged rings in the selectivity filter, and the bottom two dots in the internal entrance of the ion channel represent the dipole charges that mimic the intracellular helix dipoles of the sodium channel protein. For further details on charge types, magnitudes and positions see Section 2.1.

and length of the selectivity filter simultaneously (shape 8 and 9). We have maintained a fixed length of 54 Å for all channel shapes, as this is close to the length of the potassium channel.

2.2. Brownian Dynamics Ion Permeation Model in Sodium Channel

Figure 2 shows a schematic illustration of a BD simulation assembly for a sodium ion channel. The sodium

Table I. Nine candidates for channel shapes of the sodium ion channel considered in this paper. All dimensions are in Å (1 Å $= 10^{-10}$ meter).

	Radius			Height		
Shape	Outer vestibule	Cavity	Inner pore	Outer vestibule	Selectivity filter	Inner pore
1	14	6	4.5	10	4	28
2	8	0	0	15	0	0
3	7	6	4.5	10	8	28
4	7	6	4.5	10	4	28
5	14	6	4.5	10	8	24
6	14	6.5	6.5	10	4	27.5
7	14	6	2.5	10	4	28
8	14	8	4.5	10	4	26
9	15	8	4.5	20	4	16

ion channel is placed at the center of the assembly. The atoms forming the sodium ion channel are represented as a homogeneous medium with a dielectric constant $\epsilon p = 2$ (shaded in Fig. 2). The channel protein is assumed to have a rigid structure corresponding to the average positions of atoms forming it. Despite this necessary simplification imposed on the model, it has been shown previously that BD captures the salient conduction properties of a number of ion channels. This is because the most essential features that govern the permeation of ions across a narrow pore are captured in the model. There are minor details that can be neglected in the model for the purpose of BD simulations. For example, small variations in the radius

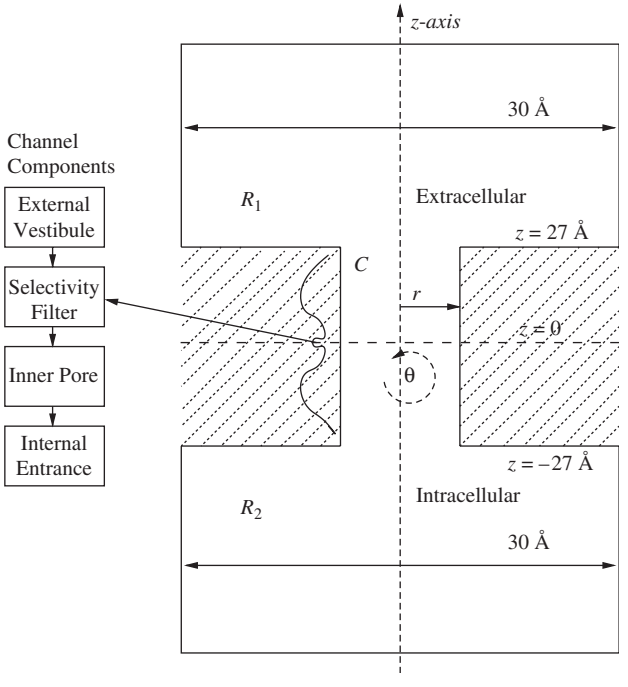

Fig. 2. Brownian dynamics model setup. The reservoir $\mathscr{R}_1$ depicts the extracellular region while the reservoir $\mathscr{R}_2$ depicts the intercellular region. As shown, the sodium ion channel comprises of 4 components. The selectivity filter is the narrowest part of the nanotube of radius $r =$ 2.2 Å. The nanotube connects the two reservoirs $\mathscr{R}_1$ and $\mathscr{R}_2$. The dark shaded region represents the protein atoms that form the ion channel.

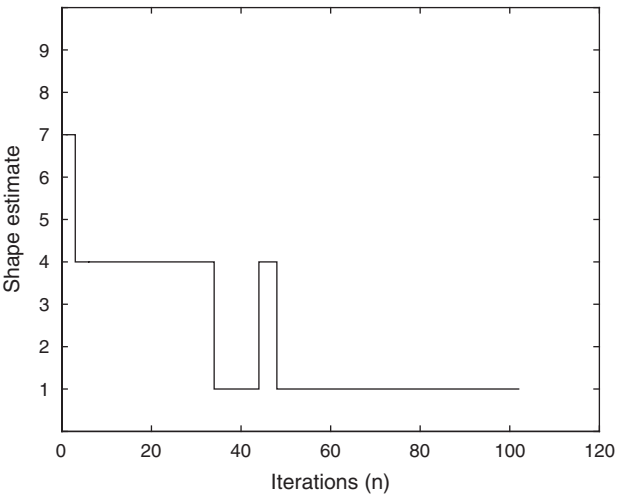

Fig. 3. Shape estimation using discrete stochastic approximation algorithm 2.

of the ion conducting pathway have no perceptible effects on electrostatic calculations and BD results. In contrast, such variations would have a drastic effect on molecular dynamics results. To carry out BD simulations of ion channels, one needs to specify the boundaries of the system. This is a relatively simple problem for 1-dimensional BD simulations,[12] but requires addition of reservoirs to the ion channel system in the more realistic case of 3-dimensional BD simulations.[14]

Two large cylindrical reservoirs denoted $\mathscr{R}_1$ and $\mathscr{R}_2$ are attached to either end of the sodium ion channel. These cylindrical reservoirs $\mathscr{R}_1$ and $\mathscr{R}_2$ in Figure 2 are each 30 Å in radius and N Å in height. To exploit the information available from known experimental measurements of the sodium ion channel current under various different conditions, such as different electrolyte solutions, concentrations and applied external voltages, we consider three distinct scenarios for the setup of the ions within the reservoirs.

Scenario 1: N positive charged Na^+ ions and N negatively charged Cl^- ions are placed in each reservoir. Each Na^+ ion has charge $q^+ = 1.6 \times 10^{-19}$ C, mass $m^{(i)} = m^+ = 3.8 \times 10^{-26}$ kg and frictional coefficient $m^+\gamma^+$, where from the Einstein–Smoluchowski relation

$$m^+\gamma^+ = \frac{kT}{D^+}, \quad D^+ = 1.33 \times 10^{-9}\ \mathrm{m^2/s} \qquad (1)$$

Here D^+ denotes the diffusion coefficient of the Na^+ ion within a bulk solution. Here $k = 1.38 \times 10^{-23}$ denotes Boltzmann's constant and T denotes the temperature in Kelvin. Na^+ ions have a radius $r^+ = 0.95$ Å. (Note: 1 Å (angstrom) $= 10^{-10}$ m.)

Each Cl^- ion has charge $q^{(i)} = q^- = -1.6 \times 10^{-19}$ C, mass $m^{(i)} = m^- = 5.9 \times 10^{-26}$ kg and frictional coefficient $m^-\gamma^- = \frac{kT}{D}$ where $D^- = 2.03 \times 10^{-9}$ m^2/s denotes the diffusion coefficient of the Cl^- ion within a bulk solution. Cl^- ions have a radius $r^- = 1.88$ Å.

Scenario 2: N positive charged Ca^{2+} (Calcium) ions and N negatively charged Cl^- (chloride) ions are placed

in each reservoir. Each Ca^{2+} ion has charge $q^{++} = 2 \times 1.6 \times 10^{-19}$ C, mass $m^{++} = 6.6 \times 10^{-26}$ kg and frictional coefficient $m^{++}\gamma^{++} = \frac{kT}{D^{++}}$ where $D^{++} = 0.79 \times 10^{-9}$ m^2/s denotes the diffusion coefficient of the Ca^{2+} ion within a bulk solution. Ca^{2+} ions have a radius $r^{++} = 0.99$ Å.

Scenario 3: N_1 Na^+ ions, N_2 Ca^{2+} ions, and N_3 Cl^- ions are placed in each reservoir. We denote $N = N_1 + N_2 + N_3$ so that the total number of ions in both reservoirs is 2_N.

For each scenario, the BD ion permeation model is constructed as follows: Let $t \geq 0$ denote continuous time. Each ion i moves in 3-dimensional space over time. Let $x_t^{(i)} = (x_t^{(i)}, y_t^{(i)}, z_t^{(i)}) \in \mathscr{R}$ and $v_t^{(i)} \in \mathbb{R}^3$ denote the position and velocity of ion i at time t.

We use $(')$ to denote transpose of a vector or matrix. The three components $x_t^{(i)}, y_t^{(i)}, z_t^{(i)}$ of $x_t^{(i)} \in \mathscr{R}$ are, respectively, the x, y, and z position coordinates. Similarly, the three components of $v_t^{(i)} \leq \mathbb{R}^3$ are the x, y, z velocity components.

At time $t = 0$, the position $x_0^{(i)}$ and velocity $v_0^{(i)}$ each of the $2N$ ions in the two reservoirs are randomly initialized as follows: Each reservoir is divided into N cells of equal volume. In each cell is placed either one Na^+, Cl^-, or Ca^{2+} ions (depending on the scenario) with equal probability. The initial position $x_0^{(i)}$ of ion i is chosen according to the uniform distribution within its cell. This initialization of $x_0^{(i)}$ emulates the BD computer software and also is necessary to ensure that two particles are not placed too close to each other. The initial velocity vectors $v_0^{(i)}$ of the $2N$ ions are initialized according to a 3-dimensional Gaussian distribution with zero mean, and 3×3 diagonal positive definite covariance matrix. Thus the distribution of the magnitude of the initial velocity $|v_0^{(i)}|$ has a Maxwell density.

From time $t = 0$ onwards, an external potential $\Phi_\Lambda^{\text{ext}}(x)$ is applied along the z axis of Figure 2, i.e., with $x = (x, y, z)$,

$$\Phi_\lambda^{\text{ext}}(x) = \lambda z, \quad \lambda \in \Lambda \tag{2}$$

Here Λ denotes a finite set of applied experimental conditions summarized in Table II.

Let $X_t = (x_t^{(1)'}, x_t^{(2)'}, x_t^{(3)'}, \ldots, x_t^{(2N)'})' \in \mathscr{R}^{2N}$ denote the positions and $V_t = (v_t^{(1)'}, v_t^{(2)'}, v_t^{(3)'}, \ldots, v_t^{(2N)'})' \in \mathbb{R}^{6N}$ denote the velocities of of all the $2N$ ions. The velocity of each individual ion evolves according to Langevin's equation (recall $i = 1, 2, \ldots, N$ denote positive ions and $i = N+1, \ldots, 2N$ denote negative ions):

$$x_t^{(i)} = x_0^{(i)} + \int_0^t v_s^{(i)} ds \tag{3}$$

$$m^+ v_t^{(i)} = m^+ v_0^{(i)} - \int_0^t m^+ \gamma^+(x_s^{(i)}) v_s^{(i)} ds + \int_0^t F_{\theta,\lambda}^{(i)}(X_s) ds + \int_0^t b^+(x_s^{(i)}) dw_s^{(i)} \tag{4}$$

$$m^- v_t^{(i)} = m^- v_0^{(i)} - \int_0^t m^- \gamma^-(x_s^{(i)}) v_s^{(i)} ds + \int_0^t F_{\theta,\lambda}^{(i)}(X_s) ds + \int_0^t b^-(x_s^{(i)}) dw_s^{(i)} \tag{5}$$

Here $\gamma(x_s^{(i)}) = \gamma$ if $x_s^{(i)} \in \mathscr{R}_1 \cup \mathscr{R}_2$, i.e., if the ion is in the reservoir, and $\gamma(x_s^{(i)})$ is determined by Molecular dynamics simulation when the ion is in the ion channel.[1] If $x_s^{(i)}$ is in the outer vestibule or selectivity filter, we have used $D^+ = 0.1$ for sodium ions, $D^{++} = 0.15$ for calcium ions and $D^- = 0.1$ for chloride ions. If $x_s^{(i)}$ is in the internal pore or internal entrance we have used $D^+ = 0.3$ for sodium ions, $D^{++} = 0.4$ for calcium ions and $D^- = 0.3$ for chloride ions.

Equation (3) merely says that velocity is the time derivative of the position. Eqs. (4) and (5) constitute the (4), (5), the process $\{w_t^{(i)}\}$ denotes a 3 dimensional Brownian motion, which is component-wise independent. The terms $b^+(x_s^{(i)})$ and $b^-(x_s^{(i)})$ are, respectively,

$$b^{+2}(x_s^{(i)}) = 2m^+\gamma^+(x_s^{(i)})kT, \quad b^{-2}(x_s^{(i)}) 2m^-\gamma^-(x_s^{(i)})kT \tag{6}$$

Thus at any time t, $b^+ w^{(i)}$ is a Gaussian random variable with zero mean ($\text{E}b^+ w_t^{(i)} = 0$), and 3×3 diagonal

Table II. Simulation conditions: simulations were performed for each shape with all twelve conditions. Concentrations inside and outside the channels were varied between solutions of NaCl and $CaCl_2$ and both. External potentials of ±70 and ±100 mV was applied.

Condition	Ion type	Φ^{ext} (mV)	Experimental $\hat{I}$(pA)	Internal concentrations (mM)	External concentrations (mM)	No. of ions in $\mathscr{R}_1$	No. of ions in $\mathscr{R}_2$
1	NaCl	+100	+2.3	200	200	14	14
2	NaCl	−100	−2.3	200	200	14	14
3	$CaCl_2$	−100	0.0	200	200	8	8
4	NaCl	−100	−0.5	200	200	12	12
	$CaCl_2$			100	100	6	6
5	NaCl	+100	+1.2	200	200	12	12
	$CaCl_2$			100	100	6	6
6	NaCl	−70	−1.6	200	200	14	14
7	NaCl	+70	+1.6	200	200	14	14
8	NaCl	−70	−1.45	100	100	10	10
9	NaCl	+70	+1.45	100	100	10	10
10	NaCl	−70	−1.65	350	350	16	16
11	NaCl	−70	−0.4	200	200	12	12
	$CaCl_2$			100	100	7	0
12	NaCl	+70	+0.9	200	200	12	12
	$CaCl_2$			100	100	0	7

covariance matrix $b^{+2}tI_{3\times3}$; similarly, $\mathrm{E}b^{-}w_t^{(i)} = 0$ and $\mathrm{E}b^{-}w^{(i)^2} = b^{-2}t\mathrm{I}_{3\times3}$. Finally, the noise processes $\{w_t^{(i)}\}$ and $\{w_t^{(j)}\}$, that drive any two different ions, $j \neq i$, are assumed to be statistically independent.

In Eqs. (4), (5), $F_{\theta,\lambda}^{(i)}(X_t) = -q^{(i)}\nabla_{x_t^{(i)}}\Phi_{\theta,\lambda}^{(i)}(X_t)$ represents the *systematic force* acting on ion i, where the scalar valued process $\Phi_{\theta,\lambda}^{(i)}(X_t)$ is the total electric potential experienced by ion i given the position X_t of the $2N$ ions. The subscript λ is the applied external potential in (2). The subscript θ is a parameter that characterizes the potential mean force (PMF) profile which is an important component of $\Phi_{\theta,\lambda}^{(i)}(X_t)$—see Section 2.3 for details.

2.3. Modeling of Systematic Force Acting on Ions

As mentioned after Eq. (5), the systematic force experienced by ion i is $F_{\theta,\lambda}^{(i)}(X_t) = q^{(i)}\nabla_{x_t^{(i)}}\Phi_{\theta,\lambda}^{(i)}(X_t)$ where the scalar valued process $\Phi_{\theta,\lambda}^{(i)}(X_t)$ denotes the total electric potential experienced by ion i given the position X_t of all the $2N$ ions. We now give a detailed formulation of these systematic forces.

The potential $\Phi_{\theta,\lambda}^{(i)}(X_t)$ experienced by each ion i comprises of the following five components:

$$\Phi_{\theta,\lambda}^{(i)}(X_t) = U_\theta(x_t^{(i)}) + \Phi_\lambda^{\mathrm{ext}}(x_t^{(i)}) + \Phi^{IW}(x_t^{(i)}) + \Phi^{C,i}(X_t) + \Phi^{SR,i}(X_t) \quad (7)$$

Note that the first three terms in Eq. (7), namely $U_0(x_t^{(i)})$, $\Phi_\lambda^{\mathrm{ext}}(x_t^{(i)})$, $\Phi^{IW}(x_t^{(i)})$ depend only on the position $x_t^{(i)}$ of ion i, whereas the last two terms in Eq. (7) $\Phi^{C,i}(X_t)$, $\Phi^{SR,i}(X_t)$, depend on the distance of ion i to all the other ions, i.e., the position X_t of all the ions. The five components in Eq. (7) are now defined.

(i) *Potential of Mean Force (PMF)* denoted $U_0(x_t^{(i)})$ in (7), comprises of electric forces acting on ion i when it is in or near the ion channel (nanotube $\mathscr{C}$ in Fig. 2). The PMF U_0 depends on the structure of the ion channel and originates from different sources, such as fixed and mobile charges and induced surface charges.

(ii) *External Applied Potential*: For ion i at position $x_t^{(i)} = x = (x, y, z)$, $\Phi_\lambda^{ext}(x) = \lambda z$ (see (2)) denotes the potential on ion i due to the applied external field. The electrical field acting on each ion due to the applied potential is therefore $-\nabla_{x_t^{(i)}}\Phi_\lambda^{\mathrm{ext}}(x) = (0, 0, \lambda)$ V/m at all $x \in \mathscr{R}$. It is this applied external field that causes a drift of ions from the reservoir $\mathscr{R}_1$ to $\mathscr{R}_2$ via the ion channel $\mathscr{C}$. As a result of this drift of ions within the electrolyte in the two reservoirs, eventually the measured potential drop across the reservoirs is zero and all the potential drop occurs across the ion channel.

(iii) *Coulomb Potential*: In Eq. (7), $\Phi^{C,i}(X_t)$ denotes the Coulomb interaction between ion i and all the other ions.

$$\Phi^{C,i}(X_i) = \frac{1}{4\pi\epsilon_0}\sum_{j=1,\,j\neq i}^{2N}\frac{q^{(j)}}{\epsilon_w\|x_t^{(i)} - x_t^{(j)}\|} \quad (8)$$

(iv) *Ion-wall Interaction Potential*: The ion-wall potential Φ^{IW} also called the *Lennard Jones potential* ensures that the position $x_t^{(i)}$ of all ions $i = 1, \ldots, 2N$ lie in $\mathscr{R}^o$. With $x_t^{(i)} = (x_t^{(i)}, y_t^{(i)}, z_t^{(i)})'$, it is modelled as

$$\Phi^{IW}(x_t^{(i)}) = \frac{F_0}{9}\frac{(r^{(i)} + r_w)^{10}}{\left[r_c + r_w - \left(\sqrt{x_t^{(i)^2} + y_t^{(i)^2}}\right)\right]^9} \quad (9)$$

where for positive ions $r^{(i)} = r^+$ (radius of Na^+ atom) and for negative ions $r^{(i)} = r^-$ (radius of Cl^- atom), $r_w = 1.4$ Å is the radius of atoms making up the wall, r_c denotes the radius of the ion channel, and $F_0 = 2 \times 10^{-10}$ N which is estimated from the ST2 water model used in molecular dynamics.[20] This Lennard-Jones potential results in short range forces that are only significant when the ion is close to the wall of the reservoirs $\mathscr{R}_1$ and $\mathscr{R}_2$ or anywhere in the ion channel $\mathscr{C}$.

(v) *Short Range Potential*: Finally, in Eq. (7)

$$\Phi^{SR,i}(X_t) = \frac{F_0}{9}\sum_{j=1,\,j\neq i}^{2N}\frac{(r^{(i)} + r^{(j)})}{\|x_t^{(i)} - x_t^{(j)}\|^9} \quad (10)$$

denotes the short range Coulomb interaction between two ions when their electron clouds overlap.

2.4. Effect of Shape on Potential of Mean Force (PMF) Profile

An ion entering the ion channel $\mathscr{C}$ experiences a force described by the first term U_θ of Eq. (7), where $\theta \in \Theta$ and $\Theta = \{S_1, S_2, \ldots, S_9\}$. One of the components of this force is the induced surface charge force. The protein has a lower dielectric constant ($\epsilon_p = 2$), compared to water ($\epsilon = 80$) the ion induced charges at the protein water boundary. These forces are repulsive, tending to push the ion away from the boundary. The magnitude of this force depends on the distance of the ion from the protein boundary. In the wider sections of the channel the induced charges would be less significant than for a narrower region of the channel. This is because in these regions the ion has more room to maneuver and finds a comfortable distance between itself and the protein boundaries. Thus, the function U_θ is very sensitive to the shape of the channel and significantly affects the current $\hat{I}_\theta$.

Once a shape has been generated, we solve Poisson's equation to obtain the potential of mean force U_θ experienced by an ion traversing the channel. This is given by,

$$\nabla^2 U_\theta(r) = -\frac{\rho_\theta(r)}{\epsilon_0\epsilon} \quad (11)$$

where $U_\theta(r)$ is the electrical potential for ion channel shape θ, $\rho_\theta(r)$, is the charge density computed from the fixed charges in the walls of the protein, the other ions in the system as well as the induced charges in the channel walls, and ϵ is the dielectric constant on either sides of the channel boundary. For complex channel shapes as this, Poisson's equation is solved numerically using the 'boundary element' method.[11,13] For further details, see Ref. [4].

Since solving Poisson's equation at each iteration of the BD simulations is computationally expensive and

time-consuming, the solution to Poisson's equation is precomputed over a spatial grid for various ion configurations and the solutions are stored in a set of 2d, 3d, and 5d lookup tables. The 2d tables store the potential arising from image forces experienced by an ion due to its presence near the membrane with a lower dielectric.

Due to the cylindrical symmetry of the channel and reservoirs, only forces for z and r have to be calculated. The 3d tables store the Coulomb interactions between the ions and fixed charges in the protein wall lining the nanotube, and the external applied potential. The 5d tables store the electric potential values for the induced charges experienced by an ion when another ion is present in the system, i.e., ion–ion interaction.

3. ADAPTIVE BROWNIAN DYNAMICS FOR ESTIMATION OF CHANNEL SHAPE

In this section we compute the optimal sodium ion channel shape θ^*. We first briefly describe the BD simulation algorithm for computing the ion channel current estimate $\hat{I}_\theta$ as a function of the candidate shape $\theta \in \Theta$.

3.1. Brownian Dynamics Algorithm for Simulating Ion Channel

To implement the BD simulation algorithm described below on a digital computer, it is necessary to discretize the continuous-time Langevin equations of the $2N$ ions. The BD simulation algorithm typically uses a sampling interval of 2×10^{-15} s for ions within the channel and a larger timestep of $\Delta = 10^{-13}$ s is used in the reservoir.

3.2. Discrete Stochastic Optimization Based Adaptive BD Simulation Algorithm

The discrete stochastic optimization controlled BD simulation algorithm described in this section is recursive and requires BD simulations on batches of data. Since the BD simulations will be conducted over batches, it is convenient to use the the index $n = 1, 2, \ldots$ to denote batch number. The aim of this section is to present efficient stochastic optimization algorithms for computing the optimal shape θ^*, where

$$\theta^* = \arg\min_{\theta \in \Theta} C(\theta) \tag{13}$$

where $\Theta = (1, 2, \ldots, S)$ denotes S feasible shapes of the sodium ion channel, and

$$C(\theta) = E\{C_n(\theta)\}, \quad C_n(\theta) = \sum_{\lambda \in \Lambda} (\hat{I}_n^{(\lambda)}(\theta) - I^{(\lambda)}(\theta))^2 \tag{14}$$

As mentioned above, Eq. (14) is a stochastic optimization problem, since we do not have a closed form expression of $C(\theta)$—instead only noisy estimates of the current $\hat{I}_n^{(\lambda)}(\theta)$ are available using BD simulation for different experimental conditions $\lambda \in \Lambda$.

Because the square error $C_n(\theta)$ is nonnegative and bounded from above, it is convenient to normalize the above optimization objective as follows: Let $\alpha < C_n(\theta) < \beta$ where α denotes a finite lower bound and $\beta > 0$ denotes a finite upper bound. For example, since $C_n(\theta)$ is nonnegative, α can be chosen as 0. Define the normalized costs $m_n(\theta)$ as

$$m_n(\theta) \stackrel{\Delta}{=} \frac{C_n(\theta) - \alpha}{\beta - \alpha}, \quad \text{where } 0 \le m_n(\theta) \le 1 \tag{15}$$

Then the optimization problem (Eq. (14)) is equivalent to

$$\theta^* = \arg\min_{\theta} m(\theta) \text{ where } m(\theta) \stackrel{\Delta}{=} E\{m_n(\theta)\} \tag{16}$$

since scaling the cost function does not affect the minimizing solution.

In the rest of this paper we will deal with the normalized discrete stochastic optimization problem (Eq. (16)) for notational convenience. Since θ^* is the global minimizer, clearly $m(\theta^*) < m(\theta)$ for $\theta \in \Theta - \{\theta^*\}$.

An obvious brute force approach for computing the optimal shape θ^* is as follows: For each possible shape $\theta \in \Theta$, run the BD simulation Algorithm 1 for a very long time sample size T and compute the estimate $m_T(\theta)$ using Eq. (15) for each possible shape θ. Finally pick $\hat{\theta}_T^* = \arg\min_{\theta \in \Theta} m_T(\theta)$. Since for any fixed θ, $m_T(\theta) \to m(\theta)$ with probability one (w.p.1) as $T \to \infty$, it follows that the brute force estimator is statistically consistent, i.e.,

$$\hat{\theta}_T^* \to \theta^* \quad \text{w.p.1 as } T \to \infty \tag{17}$$

Thus in principle, the above brute force simulation method can be used to compute the optimal channel shape. However, the method is highly inefficient since $m_T(\theta)$ needs to be evaluated for each $\theta \in \Theta$. The evaluations of $m_T(\theta)$ for $\theta \neq \theta^*$ are wasted because they contribute nothing to the estimation of the optimal shape. Indeed, the above brute force method was used manually in Ref. [22] to estimate the optimal channel shape—this took the authors several months.

The idea of discrete stochastic approximation[3] is to run more BD simulations for θ where the optimal shape is expected and less in other areas. More precisely what is

Algorithm 1 BD Algorithm for Ion Permeation

- Input parameters θ for PMF of ion channel and λ for applied experimental conditions.
- Initialize positions and velocities of all $2N$ ions according to Section 2.2.
  For discrete time $k = 1, 2, \ldots, T$ propagate the $2N$ ions according to the time discretized Brownian dynamical system.
  - If an ion crosses ion channel from $\mathcal{R}_1$ to $\mathcal{R}_2$, then update number of crossings from $\mathcal{R}_1$ to $\mathcal{R}_2$ as $L_{\mathcal{R}_1,\mathcal{R}_2} = L_{\mathcal{R}_1,\mathcal{R}_2} + 1$. Uniformly pick one ion from $\mathcal{R}_2$ and replace in $\mathcal{R}_1$.
  - If an ion crosses ion channel from $\mathcal{R}_2$ to $\mathcal{R}_1$, then update number of crossings from $\mathcal{R}_2$ to $\mathcal{R}_1$ as $L_{\mathcal{R}_2,\mathcal{R}_1} = L_{\mathcal{R}_2,\mathcal{R}_1} + 1$. Uniformly pick one ion from $\mathcal{R}_1$ and replace in $\mathcal{R}_2$.
- Compute the mean ion channel current estimate

$$\hat{I}^{(\lambda)}(\theta) = q^+ \frac{L_{\mathcal{R}_1,\mathcal{R}_2}}{T\Delta} - q^- \frac{L_{\mathcal{R}_2,\mathcal{R}_1}}{T\Delta} \tag{12}$$

RESEARCH ARTICLE

needed is a dynamic resource allocation (control) algorithm that dynamically controls (schedules) the Brownian dynamics simulation algorithm to efficiently obtain the optimal shape θ^*. We propose a discrete stochastic approximation algorithm that is both *consistent* (i.e., Eq. (17) holds) and *attracted* to the optimal shape. That is, the algorithm provably spends more time at the optimal shape gathering observations $\hat{I}^{(\lambda)}(\theta)$ at the optimal shape $\theta = \theta^*$ and less time for other shapes $\theta \in \Theta$. Thus in discrete stochastic approximation the aim is to devise an *efficient*[16] adaptive search (sampling plan) which allows to find the minimizer θ^* with as few samples as possible by not making unnecessary observations at non-promising values of θ.

In the algorithm below, the process $\{\theta_n, n = 1, 2 \ldots\}$ denotes the "state" of the algorithm. For the state θ_n, at batch time n, define the neighborhood set $\mathcal{N}_{\theta_n} = \Theta - \{\theta_n\}$. Finally, denote the S-dimensional standard unit vectors by $c_m, m = 1, \ldots, S$, where

$$e_m = [0 \ \cdots \ 0 \ 1 \ 0 \ \cdots \ 0]' \tag{18}$$

with 1 in the mth position and zeros elsewhere.

The discrete stochastic approximation algorithm we propose is as follows:

Algorithm 2 Stochastic search adaptive BD algorithm for ion channel shape estimation.

- Step 0: (Initialization.) At batch-time $n = 0$, initialize state of the algorithm $\theta_0 \in \{1, \ldots, S\}$ randomly. Initialize state occupation probabilities $\pi_0 = e_{\theta_0}$. Initialize optimal shape estimate of ion channel as $\theta_0^* = \theta_0$.
- Step 1: (Sampling and exploration.) At batch n, given current algorithm state θ_n, evaluate $m_n(\theta_n)$ according to Eq. (15) by conducting Λ independent BD simulation runs of Algorithm 1 on the ion channel. Generate an alternative candidate state $\tilde{\theta}_n$ by sampling uniformly from the neighborhood $\mathcal{N}_{\theta_0}$ of current state θ_n. Evaluate $m_n(\tilde{\theta}_n)$.
- Step 2: (Conditional acceptance test.) If $m_n(\tilde{\theta}_n) < m_n(\theta_n)$, set $\theta_{n+1} = \tilde{\theta}_n$, else, set $\theta_{n+1} = \theta_n$.
- Step 3: Update empirical state occupation probabilities π_n as
$$\pi_{n+1} = \pi_n + \mu_n(e_{\theta_{n+1}} - \pi_n), \quad \pi_0 = e_{\theta_0} \tag{19}$$
- Step 4: (Update estimate of shape of ion channel.) $\theta_n^* = \tilde{\theta}(m^*)$ where $m^* = \arg\max_{m \in \{1,\ldots,S\}} \pi_{n+1}(m)$, set $n \to n+1$, go to Step 1.

Remark: The elements $\pi_n(\theta)$ of π_n generated by Step 4 are merely normalized counters for how many times the algorithm state has visited any particular shape $\theta \in \Theta$. In particular,

$$\pi_n(\theta) = \frac{\#\text{ of times state visits shape } \theta \text{ in batches 1 to } n}{n} \tag{20}$$

is the empirical occupation probability of state θ. As we will show below, the attraction capability (efficiency) of Algorithm 2 is captured by the fact that for sufficiently larger n, $\pi_n(\theta^*) > \pi_n(\theta)$, meaning that the algorithm spends more time at the optimal shape θ^* than at any other shape $\theta \in \Theta$. As a consequence θ_n^* (which according to Step 4 is the shape at which the algorithm has spent maximum time until time n) converges to the optimal shape θ with probability one. This is formalized below.

3.2.1. Convergence of Algorithm 2

In Ref. [2], the following stochastic ordering assumption is used:

(O) For each $\theta, \tilde{\theta} \in \Theta$,

$$P(m_n(\theta^*) < m_n(\theta)) \geq P(m_n(\theta) > m_n(\theta^*))$$
$$P(m_n(\tilde{\theta}) > m_n(\theta^*)) \geq P(m_n(\tilde{\theta}) > m_n(\theta)) \tag{21}$$

Roughly speaking this assumption ensures that the algorithm is more likely to jump towards a global minimum than away from it, see Ref. [2] for details.

The following convergence theorem for Algorithm 2 is proved in Ref. [2].

Theorem 1 (Convergence and Efficiency of Algorithm 2) Under condition (O), The estimated sequence $\{\theta_n^*\}$ generated by Step 4 of Algorithm 2 converges with probability one to the global optimizer θ^*. Equivalently, Algorithm 2 is attracted to θ^* in that for sufficiently large n, the state spends more time at θ^* than any other value of $\theta \in \Theta$, i.e., the state occupation probabilities generated by Step 3 Eq. (19) satisfy $\pi_n(\theta^*) > \pi_n(\theta), \theta \in \Theta - \{\theta^*\}$.

A sufficient condition for Assumption (O) to holds (see Ref. [2].) is that the probability density functions $p_\theta(x)$ are symmetric, unimodal, and identical for all $\theta \in \Theta$. Since the distribution of the mean square error current $m_n(\theta)$ is not known, it is difficult to verify Assumption (O). However, as shown in Section 4, Algorithm 2 gives excellent numerical results for estimating the shape of the sodium ion channel.

4. NUMERICAL RESULTS—SHAPE ESTIMATION OF SODIUM ION CHANNEL

The adaptively Controlled Brownian dynamics simulation algorithms were run on the Linux Cluster LC supercomputer of the Australian National University Supercomputer Facility. This is a 800 Gflop supercomputer comprising of 152 linux nodes, each node being a Dell Precision-350 with a 2.65 GHz Pentium 4 microprocessor.

In the BD simulations we match the BD current $\hat{I}^{(\lambda)}(\theta)$ to twelve different experimental conditions $\lambda \in \Lambda$ where $\Lambda = \{\lambda_1, \ldots, \lambda_2\}$. These are described in Table II where each condition corresponds to one value for λ. The experimental current, $I^{(\lambda)}(\theta)$, used to match our simulation currents are from experimental data in Refs. [7, 17, 18] for actual sodium ion channels under different experimental conditions.

4.1. Results Using Adaptive BD Simulation

The Adaptive BD algorithms 2, were coded as Perl-Scripts. Each iteration runs 24 BD algorithms in parallel

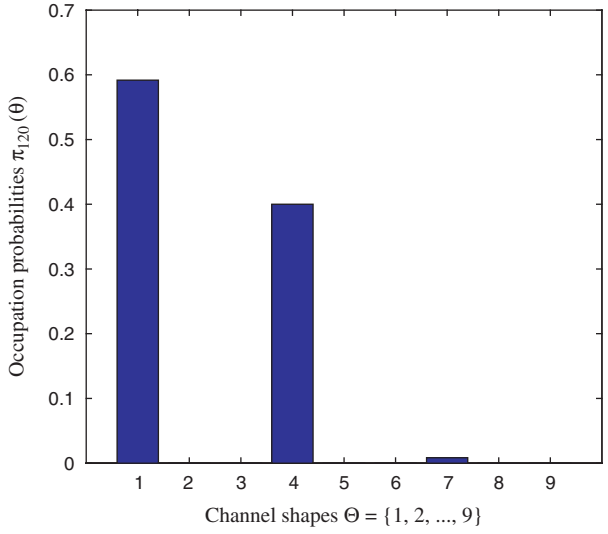

Fig. 4. Occupation probabilities of Shape Estimation Algorithm 2 after 120 iterations. These occupation probabilities $\pi(\theta_n)$ at $n = 120$ illustrate the attraction property of Algorithm 2—the algorithm spends more time near the optimal shape θ^* (Case 1) than other shape.

(12 experimental conditions for θ_n and $\tilde{\theta}_n$ in Step 1 of the adaptive BD) on the ANU supercomputer. Here we illustrate the performance of Algorithm 2 in estimating the shape of the sodium ion channel. It took approximately 38 h of simulation time to simulate all the experimental conditions $\lambda \in \Lambda$ at each $n \in N$ and a total of approximately ~4500 hrs for 120 batches. With batch jobs running in parallel, it took less than three weeks to obtain all the results.

The Figure 4 shows the estimate θ_n^* evolving versus batch iteration n for Algorithm 2. For Algorithm 2, in the initial iterations, Case 4 appears to be the best shape. However, after around $n = 60$ iterations θ_n^* converges to Case 1. Thus the optimal shape was already discernible by $n = 60$ runs but further simulations were carried out in order to be thorough.

Figure 4 plot of the empirical occupation probabilities π_n at iteration $n = 120$ for Algorithm 2. The plot illustrates the attraction property of the algorithm—it spends more time at the optimal shape (Case 1) than any other shape. The closest candidate shape to Case 1 is Case 4—and the Figures shows that the algorithm spends the second largest time at Case 4.

4.2. Interpretation of Results

At first sight, it might seem that the algorithms are not very effective in selecting an optimal shape, as there is always close competition between the two shapes $\theta = 1$ and $\theta = 4$, with $\theta = 1$ winning by only a small margin in algorithms 2. However, this calls for further inspection of the two channel models. From Table I we can see that the only difference between the two shapes is the diameter of the outer vestibule. In this region, the ions filling up this external vestibule are responsible for aiding the ions further in the selectivity filter to conduct through the channel by providing them with a repulsive kick. For shape $\theta = 1$ the width of this region is nearly 28 Å, and for shape $\theta = 4$ it is only about 14 Å. There are no other differences between the two models. We know from the paper[22] that this outer vestibule region contains on average about 2 ions during much of the BD simulation. What we have learned from this new set of simulations performed with Algorithm 2, is that, as long as the vestibule is wide enough to accommodate 2 ions, its exact width seems to be irrelevant. Once the 2 ions are present in this outer vestibule, the ions inside the channel are provided with enough repulsive force for these resident ions to move through to the other side of the channel. Thus, even though it might seem that two shapes were selected by the algorithm as being almost equally successful in satisfying all the experimental conditions presented, the important features for selectivity and permeation in the sodium channel are still maintained.

References and Notes

1. T. W. Allen, S. Kuyucak, and S. H. Chung, *Biophys. Chem.* 86, 1 (**2000**).
2. S. Andradottir, *SIAM J. Optim.* 6, 513 (**1996**).
3. S. Andradottir, *ACM Trans. Model. Computer Simula.* 9(4), 349 (**1999**).
4. S. H. Chung, T. W. Allen, M. Hoyles, and S. Kuyucak, *Biophys. J.* 77, 2517 (**1999**).
5. D. A. Doyle, J. M. Cabral, R. A. Pfuetzner, A. Kuo, J. M. Gulbis, S. L. Cohen, B. T. Chait, and R. MacKinnon, *Science* 280, 69 (**1998**).
6. R. Dutzler, E. B. Campbell, M. Cadene, B. T. Chait, and R. MacKinnon, *Nature* 415, 287 (**2002**).
7. R. J. French, J. F. Worley III, W. F. Wonderlin, A. S. Kularatna, and B. K. Krueger, *J. Gen. Physiol.* 103, 447 (**1994**).
8. H. R. Guy and S. R. Durell, Ion Channels and Diseases, The Rockefeller University Press (**1995**).
9. S. H. Heinemann, H. Terlau, W. Stühmer, K. Imoto, and S. Numa, *Nature* 356, 441 (**1992**).
10. B. Hille, *J. Gen. Physiol* 58, 599 (**1971**).
11. M. Hoyles, S. Kuyucak, and S. H. Chung, *Biophys. J.* 70, 1628 (**1996**).
12. E. Jakobbson and S. W. Chiu, *Biophys. J.* 52, 33 (**1987**).
13. D. G. Levitt, *Biophys. J.* 22, 209 (**1978**).
14. S. C. Li, M. Hoyles, S. Kuyucak, and S. H. Chung, *Biophys. J.* 74:37:47, (**1998**).
15. G. M. Lipkind and H. A. Fozzard, *Biochemistry* 39, 8161 (**2000**).
16. G. Pflug, Optimization of Stochastic Models: The Interface between Simulation and Optimization, Kluwer Academic Publishers (**1996**).
17. L. Schild and E. Moczydlowski, *Biophys. J.* 66, 654 (**1994**).
18. L. Schild, A. Ravindran, and E. Moczydlowski, *J. Gen. Physiol.* 97, 117 (**1991**).
19. T. Schlief, R. Schönherr, K. Imoto, and S. H. Heinemann, *Eur. Biophys. J.* 25, 75 (**1996**).
20. F. H. Stillinger and A. Rahman, *J. Chem. Phys.* 60, 1545 (**1974**).
21. Y. M. Sun, I. Favre, L. Schild, and E. Moczydlowsky, *J. Gen. Physiol.* 110, 693 (**1997**).
22. T. Vora, B. Corry, and S. H. Chung, *Biochimica et Biophysica Acta-Biomembranes* 1668, 106 (**2004**).

Received: XX Xxxxx XXXX. Accepted: XX Xxxxxx XXXX.

RESEARCH ARTICLE